Research, Society and Development, v. 11, n. 13, e205111335421, 2022
(CC BY 4.0) | ISSN 2525-3409 | DOI: http://dx.doi.org/10.33448/rsd-v11i13.35421

Blast-induced ground vibrations: a dynamic analysis by FEM

Vibrações induzidas por desmonte de rochas por explosivos: uma análise dinâmica via MEF

Vibraciones inducidas por voladura de rocas con explosivos: un análisis dinámico vía MEF

Received: 09/16/2022 | Revised: 09/29/2022 | Accepted: 10/26/2022 | Published: 10/05/2022

Caroline Belisário Zorzal
ORCID: https://orcid.org/0000-0001-9323-7848
Universidade Federal de Ouro Preto, Brazil
E-mail: carolinezorzal@gmail.com
Christianne de Lyra Nogueira
ORCID: https://orcid.org/0000-0002-5630-7920
Universidade Federal de Ouro Preto, Brazil
E-mail: chris@ufop.edu.br
Hernani Mota de Lima
ORCID: https://orcid.org/0000-0002-5595-4149
Universidade Federal de Ouro Preto, Brazil
E-mail: hernani.lima@ufop.edu.br

Abstract
The peak particle velocities (PPV) are fundamental for understanding and managing the levels of blast-induced ground vibrations and their effects on adjacent structures. Given that numerical analysis of seismic vibrations has been demonstrated to be a method that can significantly contribute to predicting PPV, this study adopts a numerical approach using the finite element method (FEM) to assess blasting-induced ground vibration in rock masses. A dynamic module of the stress-strain analysis based on the FEM displacement formulation is developed in ANLOG software to estimate the variations of displacement, velocity, strain, and stress induced by blasting. The dynamic modulus implemented is verified using two verification examples. After, ANLOG is used in an application example to estimate seismic vibrations induced by blasting and to define the attenuation law for a limestone quarry near an urbanized area in Spain. The effect of Rayleigh damping coefficients (α and β) on the PPV levels estimated by ANLOG was investigated, and the most appropriate numerical attenuation law is then obtained. The numerical analysis presents satisfactory results for elastic-wave propagation induced by blasting and the peak particle velocity values obtained shows good agreement with field and the numerical results available in the specialized literature. The results indicate that ANLOG can perform personalized analysis of rock mass under blast-induced dynamic stress taking into consideration the geological and geomechanical characteristics particular to each medium as well as the blast parameters.
Keywords: Blasting; Ground vibration; Finite element method; Peak particle velocities; PPV.

Resumo
As velocidades de pico de partículas (VPP) são fundamentais para entender e gerenciar os níveis de vibrações sísmicas induzidas por desmontes de rochas e seus efeitos em estruturas adjacentes. Dado que a análise numérica de vibrações tem se mostrado como um método que pode contribuir significativamente para previsão dos níveis de VPP, este estudo adota uma abordagem numérica usando o método dos elementos finitos (MEF) para avaliar as vibrações induzidas por desmontes de rocha em maciços rochosos. Um módulo dinâmico de análise tensão-deformação baseado na formulação de deslocamento do MEF foi desenvolvido no software ANLOG para estimar as variações de deslocamento, velocidade, deformação e tensões induzidas pelo desmonte de rochas. O módulo dinâmico implementado foi verificado usando dois exemplos. Em seguida, o ANLOG foi usado na estimação dos níveis de VPP e na definição da lei de atenuação de uma pedreira de calcário próxima a uma área urbanizada na Espanha. O efeito dos coeficientes de amortecimento de Rayleigh nos níveis de VPP estimados pelo ANLOG foi investigado para obter a lei de atenuação numérica mais adequada. A análise numérica apresentou resultados satisfatórios para propagação de ondas sísmicas induzidas por desmonte de rochas e os níveis de VPP obtidos mostram boa concordância com resultados de campo e numéricos disponíveis na literatura. Os resultados indicam que o ANLOG pode realizar análises personalizadas de maciço rochoso sob tensão dinâmica induzida por desmonte de rochas, levando em consideração as características geológicas e geomecânicas particulares de cada meio e os parâmetros de desmonte.
Palavras-chave: Desmonte de rochas por explosivos; Vibrações sísmicas; Método dos elementos finitos; Velocidade de pico de partícula; VPP.

Resumen
La velocidad máxima de vibración de partículas (VPP) es fundamental para gestionar las vibraciones sísmicas inducidas por voladuras de rocas con explosivos y sus efectos en las estructuras adyacentes. Dado que el análisis numérico de vibraciones ha demostrado ser un método que puede contribuir significativamente a la predicción de VPP, este estudio adopta un enfoque numérico utilizando el método de elementos finitos (FEM) para evaluar las vibraciones inducidas por voladuras en macizos rocosos. Se desarrolló un módulo de análisis dinámico de tensión-deformación basado en la formulación de desplazamiento del FEM en el software ANLOG para estimar las variaciones en el desplazamiento, la velocidad, la deformación y las tensiones inducidas por la voladura. El módulo dinámico implementado se verificó utilizando dos ejemplos. Luego, se utilizó ANLOG para estimar los niveles de VPP y definir la ley de atenuación de una mina de piedra caliza cerca de un área urbanizada en España. Se investigó el efecto de los coeficientes de amortiguamiento de Rayleigh sobre los niveles de VPP estimados por ANLOG para obtener la ley de atenuación numérica más adecuada. El análisis numérico mostró resultados satisfactorios para la propagación de ondas sísmicas inducidas por voladura de roca y los niveles de VPP obtenidos muestran una buena concordancia con los resultados numéricos y de campo disponibles en la literatura. Los resultados indican que ANLOG puede realizar análisis personalizados del macizo rocoso bajo tensiones dinámicas inducidas por voladura de rocas, teniendo en cuenta las características particulares de cada medio y los parámetros de voladura.
Palabras clave: Voladura de rocas con explosivos; Vibraciones sísmicas; Método de elementos finitos; Velocidad máxima de vibración de partículas; VPP.

1. Introduction

Blasting has been the most common excavation technique in mining engineering applications since the development of chemical blasting agents (Aydan, 2017). The blasting main objective is to fragment the largest quantity of materials at minimal cost and maximal safety. Despite all the technological advances in the mining area, only a small portion of the explosive energy is effectively used in the in-situ material fragmentation. The majority of blasting energy is used on the movement of rock fragments, heat, noise, and seismic vibrations. Concerning the stability and integrity of the rock mass and adjacent structures, the blasting-induced ground vibration has the most critical effect (Liu et al., 2017; Hu et al., 2018; Gui et al., 2018; Xu et al., 2019; Gou et al., 2020; Zorzal et al., 2022).

Regarding seismic vibrations, the blasting-induced seismic wave spreads concentrically from the blasting area and attenuates as it moves away from its source. Two distinct regions with different behaviors as identified: the near-field and the far-field region (Trigueros et al., 2017). The near-field region is the area around the blasting hole which is subjected to extremely high temperature and pressure due to chemical reactions produced by the detonation of explosives. As the shock wave moves away from the blasting hole, the rock mass is subjected to high levels of strain and experiences inelastic phenomena, such as breaking, fracturing, and crushing (Bhandari, 1997). As the shock wave attenuates, the tangential tensile stress becomes inferior to the dynamic tensile strength of the rock and an elastic behavior with no permanent strain is observed (Jimeno et al., 1995). Up to this moment, the seismic wave propagates in a far-field region. In general, this region is located around 30m away from the blasting hole depending on the blast and rock mass properties (Cervantes, 2011).

In order to quantify and evaluate the potential for seismic vibration damage it is used frequently a parameter named peak particle velocity (PPV). Different definition for the PPV can be found in the literature, but in the mining industry it is defined as the highest recorded value among the three orthogonal particle vibration components (vertical, transverse, and longitudinal or radial). Besides the PPV, some authors (Leconte, 1967 apud Jimeno et al., 1995; Ainalis et al., 2017) considers the use of the peak vector sum (PVS) defined as square root of the summed squares of velocity components at a particle time. PVS can be calculated by doing (ABNT, 2018):

$$PVS = \sqrt{V_L^{\,2} + V_T^{\,2} + V_V^{\,2}} \quad (1),$$

where V_L, V_T e V_V are, respectively, the longitudinal, transverse and vertical velocity components.

The magnitude of seismic vibrations depends on blasting parameters, geomechanical and geological parameters, and the distance between the blast and the monitoring point (Trigueros et al., 2017). The countless factors that affect the

development of vibrations are the exceptionally brief period of passage of the blast-induced seismic wave, the natural anisotropy and heterogeneity of the rock mass, and the complicated dissipation of the blasting energy. Estimating the seismic wave is very complicated whether in field or laboratory tests. Over time, several alternative initiatives have been taken to estimate the level of ground vibrations induced by blast. Empirical, statistical, mathematical, and advanced computational techniques have been developed as useful tools for studying and controlling vibration levels.

Several empirical equations with good correlation to determine the attenuation law can be found in the literature (Duvall & Petkof, 1958; Langefors & Kihlstrom, 1963; Ambraseys-Hendron, 1968; Persson et al., 1994; and others). The equation proposed by USBM (Duvall & Petkof, 1958) is one of the empirical equations established in Rock Blasting Engineering for PPV prediction, which can be written as:

$$PPV = K \times SD^{-n} \quad (2),$$

where SD is the scaled distance, and K and n are the adjustment parameters dependent on the medium characteristics and blasting plan parameters. According to Liu et al. (2017), the scaled distance can be estimated as $D/Q^{1/2}$ or $D/Q^{1/3}$, where D is the distance between the blast and the monitoring point, and Q is the maximum charge per delay. The authors indicate that $D/Q^{1/2}$ should be used for surface blasting detonations, while $D/Q^{1/3}$ for free-field explosion detonations.

From the mid-1990s, computational and technological innovations have greatly enhanced and facilitated the use of numerical simulations of complex processes, including rock blasting and its impacts. Semblat (2012) presents a review of the implementation of different linear and nonlinear numerical modeling techniques to simulate the propagation of seismic waves in one, two, and three dimensions. The seismic wave propagation in rock mass can be analyzed using numerical models based on finite differences, spectral elements, boundary elements, finite volumes, and finite elements.

The finite element method (FEM) is commonly used in evaluating blast-induced ground vibrations, either individually or coupled with other methods. The numerical approach by FEM allows monitoring, in time and space, the seismic waves. This facilitates the evaluation of the rock mass response to the induced dynamic efforts. The technique, which introduces effectiveness in dealing with complicated geometries and numerous heterogeneities in the geological medium (Semblat, 2012), has produced satisfactory outcomes compared to the traditional empirical methods and data measured in-situ (Ma et al., 1998; Toraño et al., 2006; Jommi & Pandolfi, 2008; Lu et al., 2011; Liu et al., 2017).

In this context, the numerical analysis of blast-induced ground vibrations by adopting the FEM has increased the understanding and strengthened the possibility of controlling the effects of these seismic waves on rock masses. Therefore, this manuscript proposes to assess the seismic vibrations produced by blasting through a numerical approach based on a dynamic stress-strain analysis using the homemade computational program named ANLOG (Non-Linear Analysis of Geotechnical Works; Zorzal, 2019) based on the FEM displacement isoparametric formulation. Two verification examples are used to check the dynamic modulus that was implemented, and, finally, it is used to estimate the peak particle velocities induced by blasting. The PPV values obtained from ANLOG in an application example are used to define the numerical attenuation law, which is compared with the field attenuation law.

2. Methodology: Mathematical and Numerical Formulation of the Dynamic Analysis

According to the FEM displacement isoparametric formulation, the differential equation system which represents the dynamic equilibrium of the mechanical problem, can be written in the finite element domain (V_e) as a function of the nodal displacement ($\hat{\mathbf{u}}$), velocities ($\dot{\hat{\mathbf{u}}}$), and acceleration vectors ($\ddot{\hat{\mathbf{u}}}$) as follows (Bathe, 1996):

$$\mathbf{M}_e\ddot{\hat{\mathbf{u}}} + \mathbf{C}_e\dot{\hat{\mathbf{u}}} + \mathbf{K}_e\hat{\mathbf{u}} = \mathbf{F}_e \quad (3),$$

where $\mathbf{F}_e$ is the elementary external load vector that depends on the applied surface force ($\mathbf{f}_S$) and body forces ($\mathbf{f}_B$); $\mathbf{M}_e$ is the

mass elementary matrix that depends on the material density (ρ); $\mathbf{K}_e$ is the elastic stiffness elementary matrix that depends on the Young modulus (E) and Poisson coefficient (ν); and $\mathbf{C}_e$ is the damping elementary matrix that depends on the damping property of the medium (κ).

Considering the global arrangement of all the elementary matrices, it is possible to obtain the equation of global equilibrium as

$$\mathbf{M}\hat{\ddot{\mathbf{U}}} + \mathbf{C}\hat{\dot{\mathbf{U}}} + \mathbf{K}\hat{\mathbf{U}} = \mathbf{F} \quad (4),$$

where **M**, **C**, and **K** are, respectively, the mass, damping, and stiffness global matrices; **F** is the global external load vector; and $\hat{\ddot{\mathbf{U}}}$, $\hat{\dot{\mathbf{U}}}$ and $\hat{\mathbf{U}}$ are, respectively, the global nodal acceleration, velocity, and displacement vectors.

The fact that wave energy is related to its potential for harm justifies the significance of studying seismic wave damping. In geomechanical applications, physical damping is generally taken into consideration by means of the proportional damping proposed by Rayleigh, making

$$\mathbf{C} = \alpha_R \mathbf{M} + \beta_R \mathbf{K} \quad (5),$$

where α_R and β_R are the Rayleigh damping coefficients.

It is possible estimate the damping coefficients from the following (Chopra, 2012; Clough & Penzien, 2003):

$$\alpha_R = \xi\left(2\omega_i\omega_j/(\omega_i + \omega_j)\right) \quad (6a);$$

$$\beta_R = \xi\left(2/(\omega_i + \omega_j)\right) \quad (6b);$$

where ω_i and ω_j are the natural frequencies referring to the i^{th} and j^{th} vibration modes, respectively, and ξ is the damping ratio for both the vibration modes.

It is also worth noting that in order to properly evaluate the impacts of rock blasting, it is essential to assess the dynamic nature of the pressure (P_B) acting on the blasting hole wall. As a direct measure of this pressure is difficult, theoretical approaches involving empirical formulas are essential.

In this study, the dynamic loading representing the detonation pressure function is modeled by optimizing the pressure pulse, as suggested by Saharan and Mitri (2008). The description of the pressure pulse depends on the normalized pressure values (the ratio between the applied pressure and PB) at different time instants. In their research, Saharan and Mitri (2008) present the optimized pressure profile for ideal and non-ideal detonations in 38 mm diameter blasting hole on hard brittle rocks (Figure 1).

The solution of the equation system, represented by Eq. (4), can be obtained through direct integration method and modal superposition. Cook et al. (2001) states that modal analysis is not appropriate for problems of wave propagation since a large number of frequency modes have to be determined, which will result in a high computational cost. Therefore, this work presents two direct time integration scheme: the explicit one, central difference method (CDM), and implicit one, Newmark method (NM), which are described in Table 1.

Figure 1. Optimized pressure time profile.

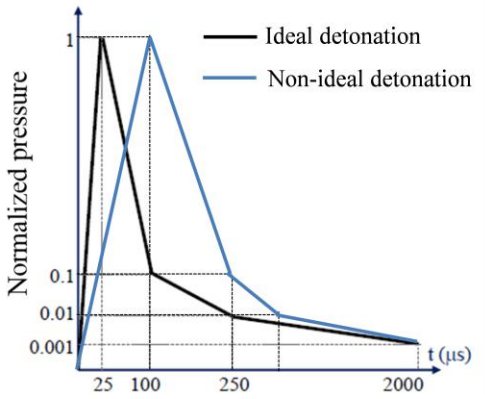

Source: Saharan and Mitri (2008).

Table 1. Direct time integration schemes (general mass and damping matrices).

A. Initial calculations:	
1. Form stiffness matrix **K**, mass matrix **M,** and damping matrix **C**	
2. Initialize $\hat{\mathbf{U}}^0$ and $\dot{\hat{\mathbf{U}}}^0$ and calculate: $\ddot{\hat{\mathbf{U}}}^0 = \mathbf{M}^{-1}\left(\mathbf{F}^0 - \mathbf{K}\hat{\mathbf{U}}^0 - \mathbf{C}\dot{\hat{\mathbf{U}}}^0\right)$	
3. Select time step	
CDM: $\Delta t \le \Delta t_{crit} = 2/\omega_n$ (ω_n is the highest natural frequency of the system)	NM: any Δt; $\delta \ge 0.5$ and $\alpha \ge 0.25(0.5+\delta)^2$
4. Calculate the integration constants	
CDM: $a_0 = 1/\Delta t^2$; $a_1 = 1/(2\Delta t)$; $a_2 = 2a_0$; $a_3 = 1/a_2$	NM: $a_0 = 1/\alpha\Delta t^2$; $a_1 = \delta/\alpha\Delta t$; $a_2 = 1/\alpha\Delta t$; $a_3 = (1/2\alpha)-1$; $a_4 = (\delta/\alpha)-1$; $a_5 = [\Delta t/2]\left[(\delta/\alpha)-2\right]$; $a_6 = (1-\delta)\Delta t$; $a_7 = \delta\Delta t$
5. Calculate $\hat{\mathbf{U}}^{-\Delta t} = \hat{\mathbf{U}}^0 - \Delta t\ \dot{\hat{\mathbf{U}}}^0 + a_3\ddot{\hat{\mathbf{U}}}^0$	
6. Form effective mass and stiffness matrixes: $\hat{\mathbf{M}} = a_0\mathbf{M} + a_1\mathbf{C}$ and $\hat{\mathbf{K}} = \mathbf{K} + \hat{\mathbf{M}}$	
B. For each time step	
7. Calculate effective load vector	
CDM at time t: $\hat{\mathbf{F}}^t = \mathbf{F}^t - (\mathbf{K} - a_2\mathbf{M})\hat{\mathbf{U}}^t - (a_0\mathbf{M} - a_1\mathbf{C})\hat{\mathbf{U}}^{t-\Delta t}$	NM at time t+Δt: $\hat{\mathbf{F}}^{t+\Delta t} = \mathbf{F}^{t+\Delta t} + \mathbf{M}\left(a_0\hat{\mathbf{U}}^t + a_2\dot{\hat{\mathbf{U}}}^t\mathbf{K} + a_3\ddot{\hat{\mathbf{U}}}\right) - \mathbf{C}\left(a_1\hat{\mathbf{U}}^t + a_4\dot{\hat{\mathbf{U}}}^t\mathbf{K} + a_5\ddot{\hat{\mathbf{U}}}\right)$
8. Solve for displacement at time t+Δt:	
CDM: $\hat{\mathbf{M}}\hat{\mathbf{U}}^{t+\Delta t} = \hat{\mathbf{F}}^t$	NM: $\hat{\mathbf{K}}\hat{\mathbf{U}}^{t+\Delta t} = \hat{\mathbf{F}}^t$
9. Calculate the acceleration and velocities	
CDM at time t: $\ddot{\hat{\mathbf{U}}}^t = a_0\left(\hat{\mathbf{U}}^{t-\Delta t} - 2\hat{\mathbf{U}}^t + \hat{\mathbf{U}}^{t+\Delta t}\right)$; $\dot{\hat{\mathbf{U}}}^t = a_1\left(-\hat{\mathbf{U}}^{t-\Delta t} + \hat{\mathbf{U}}^{t+\Delta t}\right)$	NM at time t+Δt $\ddot{\hat{\mathbf{U}}}^{t+\Delta t} = a_0\left(\hat{\mathbf{U}}^{t+\Delta t} - \hat{\mathbf{U}}^t\right) - a_2\dot{\hat{\mathbf{U}}}^t - a_3\ddot{\hat{\mathbf{U}}}^t$; $\dot{\hat{\mathbf{U}}}^{t+\Delta t} = \dot{\hat{\mathbf{U}}}^t + a_6\ddot{\hat{\mathbf{U}}}^t + a_7\ddot{\hat{\mathbf{U}}}^{t+\Delta t}$

Source: Bathe (1996).

3. Results and Discussion

3.1 Verification examples

Two examples are presented in this item in order to check the dynamic modulus implemented into ANLOG by analyzing a one-dimensional problem of wave propagation in a homogeneous and elastic medium without dissipative forces (**C≡0**). The first example shows the displacement variation throughout a free-fixed column under harmonic loading on its top (Figure 2a). The second one deals with the time and space variation of the displacements and velocities experienced by a cantilever beam under heaviside loading (Figure 2b).

Figure 2. Verification examples.

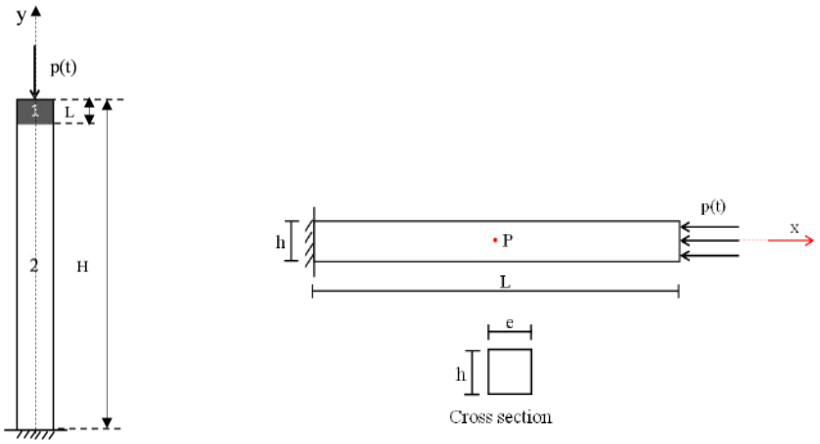

a) Free-fixed column under harmonic loading

b) Cantilever beam under Heaviside load

Source: Authors.

Example 1

A column with total length (L) of 1.0m and cross section (A) of $4.0x10^{-4}$ m^2, is composed by two different material with linear elastic behavior neglecting the damping property. The material 1 represents the colunm chapiter of 0.5m length (L) with Young Modulus (E) of 200GPa, density (ρ) of 7.8t/m^3. The material 2 represents the colunm body with Young Modulus (E) of 4.432MPa, density (ρ) of 1.56t/m^3. The column is subject to a harmonic loading on its top defined as:

$$p(t) = -P_0 sen(\omega t) \quad (7),$$

in which P_0 and ω are the magnitude and frequency of 4N ($4x10^{-3}$KN) and 150 rad/s, respectively.

This problem was studied by Bathe (1996) by considering the column as a circular cross section bar subject to a time dependent load and neglecting the body force action. Figure 3 presents the axial displacement distribution along the column at the time instant of 0.01s after the loading application by considering the CDM and NM direct integration schemes.

As the central difference method is conditionally stable the increment of $2x10^{-6}$ s was adopted. This time increment is lower than the critical time increment of $2.96x10^{-6}$s obtained by adopting the highest natural frequency of $6.77x10^5$ rad/s for a finite element mesh consists of 40 one dimensional linear elements (B2) with the same size.

The Newmark method is unconditionally stable, so the time increment of $5.0x10^{-5}$ s was adopted with the values of 0.5 and 0.25, respectively, for parameters δ and α (Table 1).

As it can be seem in Figure 3, the ANLOG and Bathe (1996) results are in a good agreement and there is no difference between the time integration schemes. However, it is important to state that Newmark method presents lowest computational cost since the time processing was 1.67s while the time processing of the central difference method was 40.69s.

Figure 3. Axial displacement distribution (t=0.01s): influence of the direct time integration scheme.

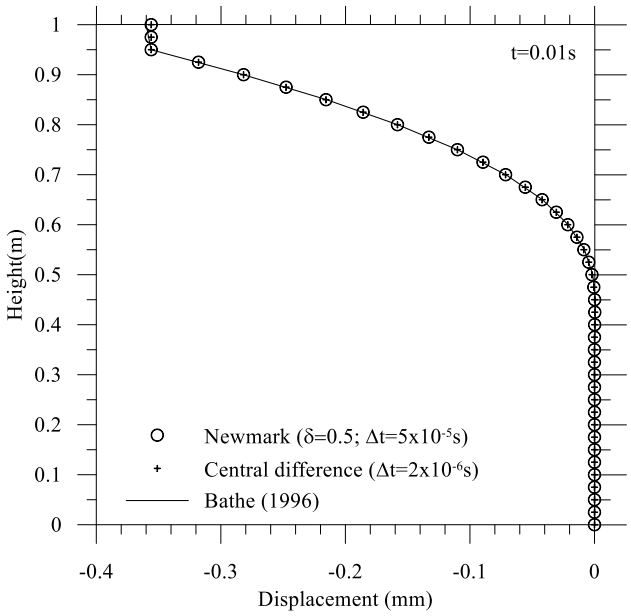

Source: Authors.

Example 2

The cantilever beam depicted in Figure 2b has a length (L) of 1.0m and a rectangular cross section (A) with height (h) and width (e) of 0.1m. The beam presents a Young Modulus (E) of 56.4GPa, density (ρ) of 2.7t/m^3 and neglected damping (κ=0). The beam is subject to a Heaviside step function at its free extremity given by:

$$p(t) = P_0 H(t) \tag{8},$$

in which

$$H(t) = \begin{cases} 0 & \text{para} \quad t < 0 \\ 1 & \text{para} \quad t \geq 0 \end{cases} \tag{9},$$

where P_0 is the load magnitude, adopted as -100kN.

The analytical solution (Clough & Penzien, 2003) in terms of longitudinal displacement (u) and velocity (v), is, respectively, given by:

$$u(x,t) = u_0 \sum_{n=1}^{\infty} \left\{ \left[(-1)^{n-1} / m^2 \right] \text{sen}\left\{ [m/2](\pi x/L) \right\} \left[1 - \cos\left\{ [m/2L]\pi ct \right\} \right] \right\} \tag{10},$$

$$v(x,t) = u_0 \sum_{n=1}^{\infty} \left\{ \left[(-1)^{n-1} / m^2 \right] \text{sen}\left\{ [m/2L]\pi x \right\} \left\{ [m/2L]\pi c \right\} \text{sen}\left\{ [m/2L]\pi ct \right\} \right\} \tag{11},$$

in which

$$u_0 = 8P_0 L / \pi^2 EA \tag{12},$$

$$m = 2n - 1 \tag{13},$$

where c is the wave velocity, defined as 4570.44 m/s for the analyzed material.

This problem was solved numerically by using ANLOG program adopting the Newmark method considering the values of 0.625 and 0.316, respectively, for parameters δ and α. The finite element mesh (Figure 4a) consists on 50 quadrilateral quadratic elements (Q8; Nogueira, 1998) with the same size and 253 nodal points. Figure 4b and Figure 4c presents the analytical (Clough & Penzien, 2003) and numerical results (ANLOG) in terms of the displacement and velocity at

point P, which is located in the middle of the beam (Figure 2b). As it can be seen, the numerical results obtained by ANLOG are in a good agreement with the solutions obtained analytically.

Figure 4. Evolution in time of the longitudinal displacement and velocity at the P point.

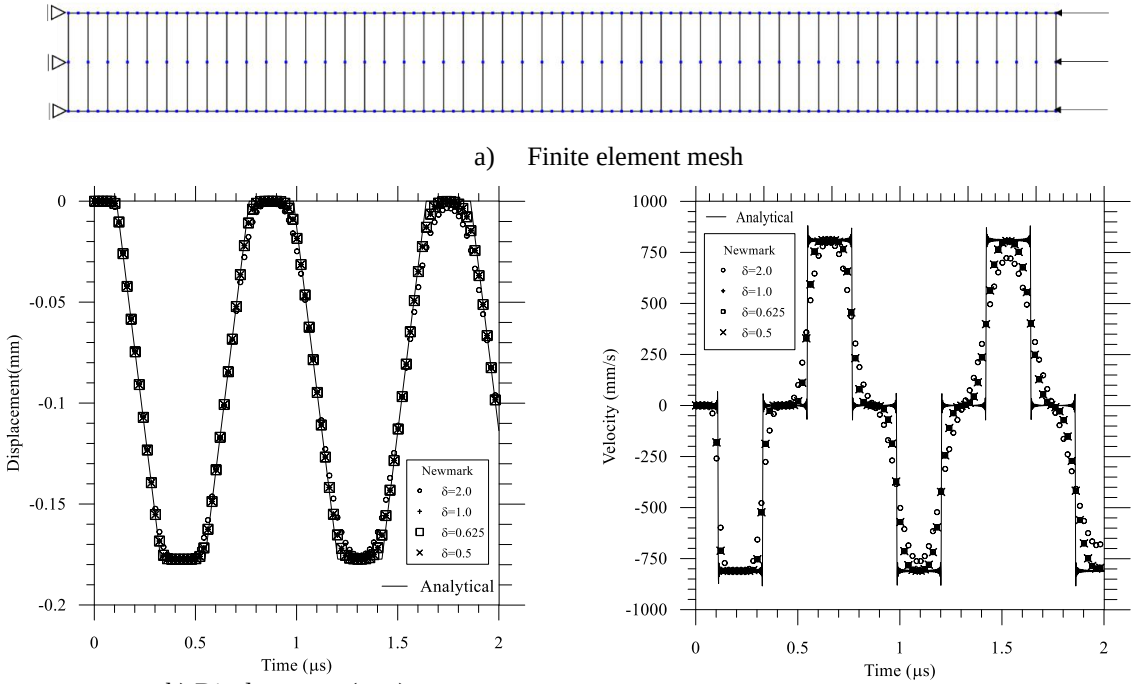

a) Finite element mesh

b) Displacement (mm)

c) Velocity (mm/s)

Source: Authors.

3.2 Application example

In this application example, ANLOG is used to estimate seismic vibrations induced by blasting in a rock mass consisting of limestone with density (ρ) of 2.6t/m^3, Young Modulus (E) of 12GPa, and Poisson coefficient (ν) of 0.2. The rock mass is subjected to an optimized pressure pulse (Saharan & Mitri, 2008) as depicted in Figure 1. The PPV values obtained from ANLOG are used to define the numerical attenuation law, which is compared with the in-situ attenuation law (Toraño et al., 2006) from a limestone quarry located near an urbanized area in Spain.

The 20m deep blast hole, which corresponds to the bench height (H_B), was loaded with 100kg of explosives. The blasting produced a peak borehole pressure (P_B) with estimated magnitude of 28MPa (Toraño et al., 2006). Although the authors did not explain the type of explosive used, this analysis was carried out using the optimized pressure pulse for non-ideal detonation. According to the specialized literature, this type of explosive is commonly used in quarry detonation operations (Cardoso, 2011; Munaretti, 2002; Koppe & Costa, 2012).

Figure 5 presents the finite element mesh and the boundary conditions adopted to analyze the problem in plane strain condition. The study area has a length (L) of 600m and a depth (H) of 150m. These values were arbitrated to prevent the development of spurious wave reflections in the boundary domain. The finite element mesh consists of 396 Q8 elements and 1289 nodes. The sizes of the elements vary from 5x5m near the application point of the detonation charge to 50x50m at the most distant points. The peak particle velocity values were collected at the surface points P_1, P_2, P_3, P_4, P_5, P_6, P_7, P_8, P_9, P_{10}, P_{11}, P_{12}, P_{13}, and P_{14}, respectively, at 30m, 50m, 75m, 125m, 150m, 175m, 200m, 250m, 300m, 350m, 400m, 450m, and 500m distance from the blasting front, as shown in Figure 5.

Figure 5. Finite element mesh and boundary conditions at a limestone quarry.

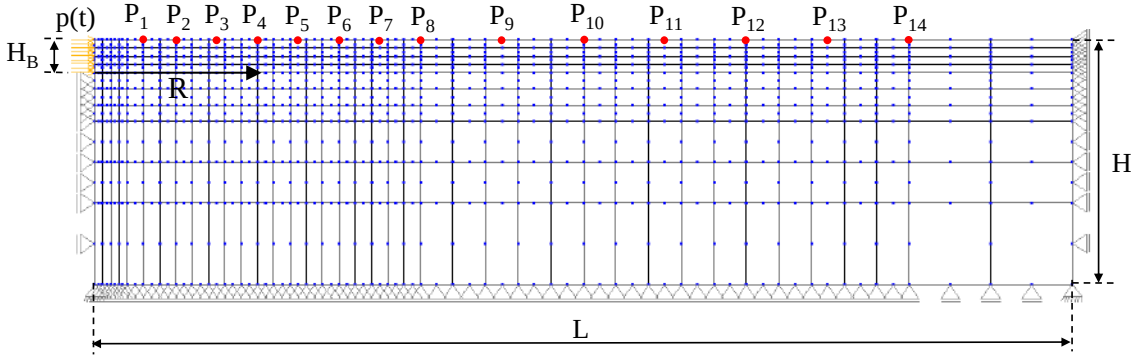

Source: Authors.

The Newmark algorithm was adopted with values of 0.316 and 0.625, respectively, for α and δ parameters. A time of 0.3s was evaluated as the travel time of the seismic wave, produced by the detonation, to reach a distance of 400m from the blast hole. The time evolution took place in two blocks. The first block consisted of 40 equal time increments of $5.0x10^{-5}$s until the time instant of $2x10^{-3}$s to be able to capture the pressure pulse variation over time. The second block comprised of 2980 equal time increments of 10^{-4}s until the time instant of 0.3s. By increasing the time increment, the computational cost can be reduced.

The Rayleigh damping method (Equation 5) was adopted to simulate the effect of physical damping, since it is a common practice in the context of elastic analysis in geomechanical applications. The natural frequencies (ω_i and ω_j) selected for the calculation of α_R (Equation 6a) and β_R (Equation 6b) were, respectively, 135.57 and 147.28rad/s. These correspond to the lower natural frequencies for the finite element mesh and material properties taken in this problem. The damping ratio for geological materials varied between 2 and 5%, as proposed by several authors (Biggs, 1964; Babanouri et al., 2013; Azizabadi et al., 2014; Gui et al., 2017). Thus, by varying the damping ratio, different values were obtained for the Rayleigh coefficients (Table 2).

Table 2. Values α_R and β_R calculated from damping factor and natural frequencies.

ξ (%)	**ω_i (rad/s)**	**ω_j (rad/s)**	α_R	β_R
2.0	135.57	147.28	2.82	$1.4x10^{-4}$
2.5	135.57	147.28	3.53	$1.8x10^{-4}$
3.0	135.57	147.28	4.24	$2.1x10^{-4}$
3.5	135.57	147.28	4.94	$2.5x10^{-4}$
4.0	135.57	147.28	5.65	$2.8x10^{-4}$
4.5	135.57	147.28	6.35	$3.2x10^{-4}$
5.0	135.57	147.28	7.06	$3.5x10^{-4}$

Source: Authors.

The numerical attenuation curve is obtained by plotting the PPV values as a function of the scaled distance (SD) defined as $D/Q^{1/2}$ (ABNT, 2018; Liu et al., 2017; Gou et al., 2020). Figure 6 shows the attenuation curves obtained as a function of the damping ratios (ξ) (Table 2). As expected, there is a decrease in the PPV levels with a rise in the damping ratio. Noteworthy is that the numerical attenuation curve nearest to the field attenuation curve acquired by Toraño et al. (2006) is the one in which the damping ratio is 2.5%. Therefore, the values of 3.53 for α_R and $1.8x10^{-4}$ for β_R were taken as reference to evaluate the impact of the Rayleigh coefficients on the numerical attenuation law.

Figure 6. Attenuation curves as a function of damping ratio (ξ).

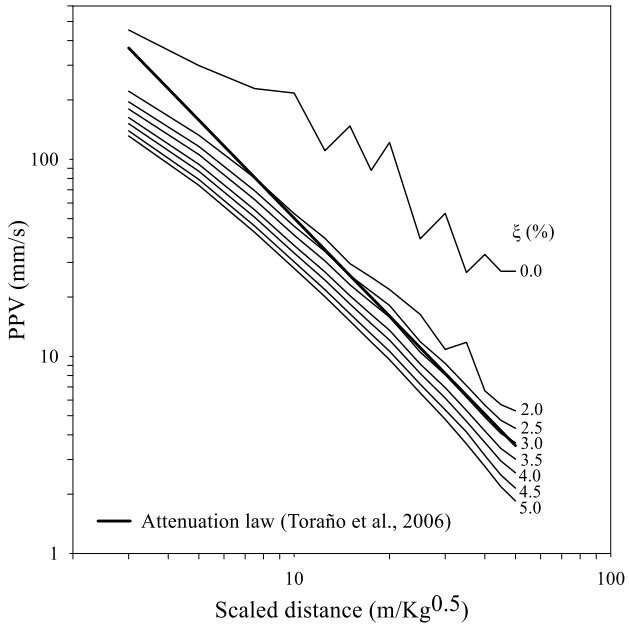

Source: Authors.

Adopting the damping ratio as 2.5%, a sensitive analysis was performed. Figure 7a demonstrates that while maintaining the α_R value as constant and increasing the β_R value, the PPV levels decrease. It is also observed that there is a presence of a characteristic noise of the numerical simulation for the smaller values of β_R ($0.5x10^{-4}$ and $1.0x10^{-4}$). As the values of β_R rise, these noises are dampened, confirming that β_R has the ability to dampen high frequencies of non-physical vibrations, that is, the noise derived from numerical simulation (Cook et al., 2001). Figure 7b demonstrates the value of α_R affects vibration attenuation as the seismic wave moves away from the point of origin. It can be noted that the vibration attenuation at distant points is more intense while keeping β_R constant and increasing the value of α_R.

Knowing the influence of the Rayleigh coefficients on the results obtained, it can be said that the numerical attenuation law converges to the field attenuation law (Toraño et al., 2006) with the values of $\alpha_R = 10.0$ e $\beta_R = 1.1x10^{-4}$. The field attenuation curve and the results produced by the Algor program (Toraño et al., 2006), as well as the results obtained by ANLOG, are shown in Figure 8. In general, it is possible to affirm that the numerical findings acquired are similar to those predicted by the attenuation law.

Figure 7. Numerical attenuation curves in function of the Rayleigh coefficients.

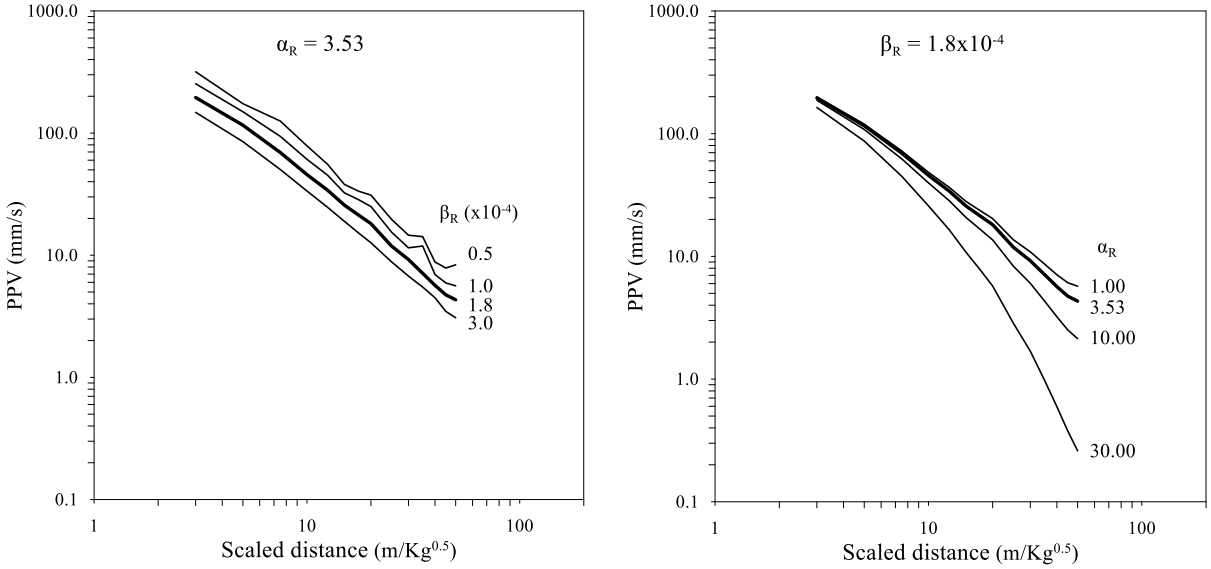

(a) Influence of β_R on the attenuation curve. (b) Influence of α_R on the attenuation curve.

Source: Authors.

Figure 8. Attenuation law (Field versus Numericals).

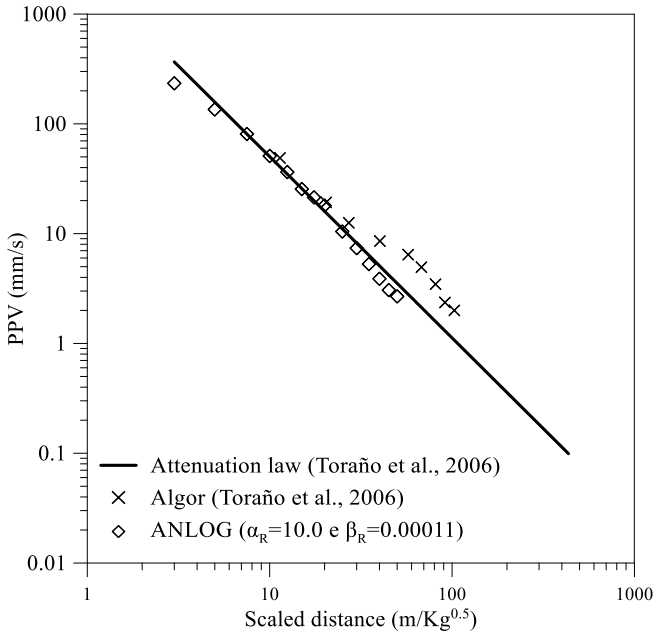

Source: Authors.

In order to determine the most appropriate parameter to define the attenuation law, the PPV and PVS estimated by ANLOG are plotted as a function of scaled distance in Figure 9. The results showed that there is no significant difference between the numerical attenuation laws for both parameters in the situation under consideration (plane strain analysis). This suggests that both PPV and PVS can be used as parameters to estimate the attenuation law, as Gou et al. (2020) also observed in blast-induced ground vibrations analysis in an underground mine.

Figure 9. PVS and PPV fitted equation.

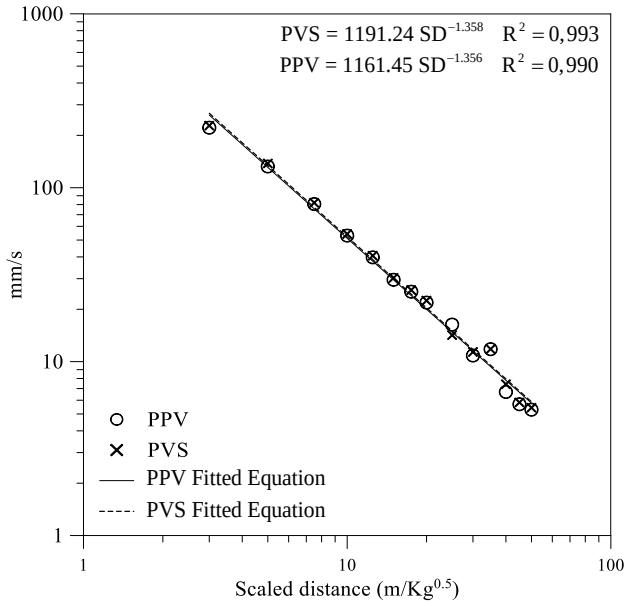

Source: Authors.

4. Conclusion

In this paper, the blast-induced ground vibrations were assessed through a numerical approach based on a dynamic stress-strain analysis using the homemade computational program named ANLOG based on the FEM displacement isoparametric formulation. The mathematical and numerical formulations developed in the ANLOG software to solve the dynamic problem were first presented. Two verification examples were used to check the dynamic modulus that was implemented.

The application problem presented showed the importance of the Rayleigh coefficients on the numerical results. The findings imply that in a plane strain study, both PPV and PVS can be employed as parameters to determine the attenuation law. As a result, PPV was chosen in this study since it has the lowest computing cost. In general, it is possible to affirm that the numerical attenuation law acquired by ANLOG are similar to those predicted by the field attenuation law.

The present work showed the importance of dynamic stress-strain analysis to obtain blast-induced ground vibrations. Furthermore, the results demonstrated the ability of the ANLOG program to in individualized rock mass analysis under blast-induced dynamic stress, taking into account the geological and geomechanical parameters specific to each medium as well as the blast parameters, at reasonable speed and low cost.

Continuing this work, the following interventions are suggested: Implementing mass matrices and damping for three-dimensional issues; examining additional simulation models of the detonation pressure function; taking into account the material's constitutive nonlinearity in numerical modelling; create a module for vibration frequency analysis; assess the impact of blast-induced ground vibrations on natural underground cavities.

Acknowledgments

This study was financed in part by the Coordenação de Aperfeiçoamento de Pessoal de Nível Superior - Brasil (CAPES) - Finance Code 001. The authors would like to thank CAPES, CNPq, FAPEMIG, Fundação Gorceix, PPGEM/UFOP, PROPEC/UFOP, and PROPP/UFOP for their financial support. The first author would like to thank CAPES for their grant.

References

ABNT NBR 9653. (2018). *NBR 9653: Guia para avaliação dos efeitos provocados pelo uso de explosivos nas minerações em áreas urbanas* – Procedimento. Rio de Janeiro.

Ainalis, D., Kaufmann, O., Tshibangu, J. P., Verlinden, O., & Kouroussis G. (2017). Modelling the Source of Blasting for the Numerical Simulation of Blast-Induced Ground Vibrations: A Review. *Rock Mechanics and Rock Engineering*, 50(1):171-193.

Ambraseys, N. R., & Hendron, A. J. (1968). *Dynamic behaviour of rock masses: rock mechanics in engineering practices*. Wiley, London.

Aydan, O. (2017). *Rock dynamics*. CRC Press/Balkema, London.

Azizabadi, H. R. M., Mansouri, H., & Fouché, O. (2014). Coupling of two methods, waveform superposition and numerical, to model blast vibration effect on slope stability in jointed rock masses. *Computers and Geotechnics*, 61:42–9.

Babanouri, N., Mansouri, H., Nasab, S. K., & Bahaadini, M. (2013). A coupled method to study blast wave propagation in fractured rock masses and estimate unknown properties. *Computers and Geotechnics*, 49:134–42.

Bathe, K. J. (1996). *Finite element procedures*. Prentice-Hall Inc., New Jersey.

Bhandari, S. (1997). *Engineering rock blasting operations*. A. A. Balkema Publishers, Rotterdam/Brookfield.

Biggs, J. M. (1964). *Introduction to structural dynamics*. McGraw-Hill, New York.

Cardoso, E. R. (2011). *Simulação numérica da detonação de explosivos não ideais*. [Doctoral dissertation, Universidade de Coimbra].

Cervantes, L. M. T. (2011). *Resistência de maciços rochosos estruturalmente complexos de mineração submetidos a carregamentos dinâmicos*. [Doctoral dissertation, Universidade de Brasília].

Chopra, A. K. (2012). *Dynamics of structures*. (4th ed.) Prantice-Hall, Boston.

Clough, R. W., & Penzien, J. (2003). *Dynamics of structures*. (3th ed.) Computers & Structures Inc., Berkeley.

Cook, R. D., Malkus, D. S., Plesha, M. E., & Witt, R. J. (2001). *Concepts and applications of finite element analysis*. (4th ed.) John Willeys & Sons Inc., Madison.

Duvall, W. I., & Petkof, B. (1959). Spherical propagation of explosion generated strain pulses in rock. *USBM RI 5483*.

Gou, Y., Shi, X., Zhou, J., Qiu, X., Chen, X., & Huo, X. (2020). Attenuation assessment of blast-induced vibrations derived from an underground mine. *International Journal of Rock Mechanics and Mining Sciences*, 127:104220.

Gui, Y. L., Zhao, Z. Y., Jayasinghe, L. B., Zhou, H. Y., & Tao, M. (2018). Blast wave induced spatial variation of ground vibration considering field geological conditions. *International Journal of Rock Mechanics and Mining Sciences*, 101:63-68.

Gui, Y. L., Zhao, Z. Y., Zhou, H. Y., Goh, A. T. C., & Jayasinghe, L. B. (2017). Numerical Simulation of Rock Blasting Induced Free Field Vibration. *Procedia Engineering*, 191:451–7.

Hu, L., Liu, M., Wu, X., Zhao, G., & Li, P. (2018). Damage-vibration couple control of rock mass blasting for high rock slopes. *International Journal of Rock Mechanics and Mining Sciences*, 103:137-144.

Jimeno, C. L., Jimeno, E. L., & Carcedo, F. J. A. (1995). *Drilling and blasting of rocks*. A. A. Balkema Publishers, Rotterdam/Brookfield.

Jommi, C., & Pandolfi, A. (2008). Vibrations induced by blasting in rock: a numerical approach. *Rivista Italiana di Geotecnica*, 20:77–94.

Koppe, J. C., & Costa, J. F. C. L. (2012). Operações de lavra em pedreiras. In: Luz, A. B., & Almeida, S. L. M. (eds) *Manual de agregados para construção civil*. (2th ed.) CETEM, Rio de Janeiro, 127-164.

Langefors, U., & Kihlstrom, B. (1963). *The modern technique of rock blasting*. Wiley, New York.

Liu, K., Hao, H., & Li, X. (2017). Numerical analysis of the stability of abandoned cavities in bench blasting. *International Journal of Rock Mechanics and Mining Sciences*, 92:30-39.

Lu, W., Yang, J., Chen, M., & Zhou, C. (2011). An equivalent method for blasting vibration simulation. *Simulation Modelling Practice and Theory*, 19:2050–62.

Ma, G. W., Hao, H., & Zhou, Y. X. (1998). Modeling of wave propagation induced by underground explosion. *Computers and Geotechnics*, 22:283–303.

Munaretti, E. (2002). *Avaliação da utilização de AN/FO fabricado in situ em pedreira de calcário*. [Master's thesis, Universidade Federal do Rio Grande do Sul].

Nogueira, C. L. (1998). *Análise não linear de escavações e aterros*. [Doctoral dissertation, Pontifícia Universidade Católica do Rio de Janeiro].

Persson, P. A., Holmberg, R., & Lee, J. (1994). *Rock blasting and explosives engineering*. CRC Press, Boca Raton.

Saharan, M. R., & Mitri, H. S. (2008). Numerical procedure for dynamic simulation of discrete fractures due to blasting. *Rock Mechanics and Rock Engineering*, 41:641–70.

Semblat, J. F. (2012). Modeling seismic wave propagation and amplification in 1D/2D/3D linear and nonlinear unbounded media. *International Journal of Geomechanics*, 11:440–8.

Toraño, J., Rodríguez, R., Diego, I., Rivas, J. M., & Casal, M. D. (2006). FEM models including randomness and its application to the blasting vibrations prediction. *Computers and Geotechnics*, 33:15–28.

Trigueros, E., Cánovas, M., Muñoz, J. M., & Cospedal, J. (2017). A methodology based on geomechanical and geophysical techniques to avoid ornamental stone damage caused by blast-induced ground vibrations. *International Journal of Rock Mechanics and Mining Sciences*, 93:196–200.

Xu, J., Kang, Y., Wang, X., Feng, G., & Wang, Z. (2019). Dynamic characteristics and safety criterion of deep rock mine opening under blast loading. *International Journal of Rock Mechanics and Mining Sciences*, 119:156-167.

Zorzal, C. B. (2019). *Análise dinâmica via MEF das vibrações induzidas pelo desmonte de rochas*. [Master's thesis, Universidade Federal de Ouro Preto].

Zorzal, C. B., Santos, F. L., Silva, J. M., & Souza, R. F. (2022). Predição de vibrações induzidas por desmontes de rochas por explosivos usando redes neurais artificiais. *Research, Society and Development*, 11 (11), e576111134020.10.33448/rsd-v11i11.34020